SUPPLEMENTARY MATERIAL

MATERIALS AND METHODS

Primary Antibodies and chemicals

The following commercial primary antibodies (Abs) were used in this study: mouse anti-βIII-tubulin (Covance); mouse anti-α-tyrosinated-tubulin, mouse anti-α-acetylated tubulin, mouse anti-α-tubulin, mouse anti-β-actin and rabbit anti-GST (Sigma-Aldrich); mouse anti-α-detyrosinated (Glu)-tubulin, rat anti-EB3 and rabbit-anti-Myc (Abcam); goat anti-MAP1B (N-t, N19), goat anti-tau (C-t, C-17) and mouse anti-GFP (Santa Cruz Biotechnology); mouse anti-EB1 (BD Transduction) and mouse anti-His tag (Millipore). We also used the previously described Abs: anti-CLIP-170 (#2360, (Coquelle et al., 2002)), anti-CLIP-115 (#2238) and anti-CLIP-115/CLIP-170 (#2221), (Hoogenraad et al., 2000) and #02-1005-07 against EB3 (Stepanova et al., 2003). A pool of anti-CLIPs was used in primary neurons (#2360+#2238+#2221). Kinase inhibitors used were: Lithium chloride, DMAT and Roscovitine (Sigma-Aldrich).

Plasmids and transfection

Previously described EB3-mCherry and GFP-tagged EB1 or EB3 expression constructs (N-t or C-t tagged) were used (Komarova et al., 2002; Stepanova et al., 2003). MAP1B-GFP was a gift of Dr. J.A. Esteban; MAP1B-Myc and MAP1B 1-508-Myc were gifts of Dr. F. Propst and pLV-GFP-tau42 (designated as GFP-tau in the text) was a gift of Dr. I. Santa-Maria. NIE-115 cells were transfected using Lipofectamine 2000 (Invitrogen) based on the manufacturer's protocol, with the indicated plasmid(s) for 36 h.

shRNA lentiviral constructs

Different MAP1B and tau shRNA lentiviral constructs (Mission, Sigma-Aldrich) were used: **MAP1B**: **shRNA1**$_{(TRCN0000091919)}$:$_{5'}$CCGGGCCGAGTTAGACATCAAAGATCTCGAGA

TCTTTGATGTCTAACTCGGCTTTTTG3´;**shRNA2**:(TRCN0000091921):5´CCGGCGGATTCAACA TGCTCATCAACTCGAGTTGATGAGCATGTTGAATCCGTTTTTG3´;**shRNA3**(TRCN0000091922) ;5´CCGGGCCCAAGAAAGAAGTGGTTAACTCGAGTTAACCACTTCTTTCTTGGGCTTTT TG3´;**tau**:**shRNA1**(TRCN0000091300):5´CCGGGACAGAGTCCAGTCGAAGATTCTCGAGAATCT TCGACTGGACTCTGTCTTTTTG3´:**shRNA2**(TRCN0000091301):5´CCGGCCTAAAGAATGTAGG GTCGAACTCGAGTTCGACCCTACATTCTTTAGGTTTTTG3´. A scramble (non-targeting) shRNA construct was used as a control.

Co-Immunoprecipitation (Co-IP) and Western blotting

Cells were harvested in cold lysis buffer and centrifuged at 13.000 rpm for 15 minutes, and the supernatant was considered as the total cell lysate. Lysis buffer contained 20 mM Tris-HCl (pH 7.5), 100 mM NaCl, 1mM ortovanadate, 1mm okadaic acid, 0.5 % Triton X-100, supplemented with 1× CompleteTM protease inhibitor cocktail (Roche). All subsequent steps were carried out at 4°C. Co-IPs were performed in each case from 500 μg of total protein extracts, using the ExactaCruz kit (Santa Cruz Biotechnology), following the manufacturer's protocol. Immunocomplexes were subjected to SDS-PAGE and Western blotting. Proteins (25-50 μg) were separated by SDS-PAGE and transferred to nitrocellulose filters. The filters were blocked with 10% non-fat milk powder or 5% BSA in phosphate-buffered saline (PBS)-0.1% Tween 20 (PBS-T), and subsequently incubated with primary antibodies overnight (4°C), followed by incubation with the corresponding peroxidase-conjugated secondary antibody (DAKO, Carpinteria, CA) for 1 h. Immunoreactivity was visualized by enhanced chemiluminescence detection (ECL, Amersham).

Bacterial expression constructs

GST-tagged fusions of EB1 and EB3 were described previously (Komarova et al., 2005). 6xHis-tagged N-terminal fragment of MAP1B (aa 1-508) was a gift of F. Propst.

GST and His fusion proteins were induced in BL21 *E. coli*, as described (Smith and Johnson, 1988) and purified on glutathione-Sepharose 4B beads (GE Healthcare) and Ni-NTA agarose beads (Qiagen) respectively, according to the instructions of the manufacturer.

Image processing

Image J free software was used to quantify EB comet number, length and fluorescence intensity profile. EB1/3-highlighted comets were counted in delimited cell areas of 100μm^2. EB1/3-comet lengths were defined as the distances from the peak fluorescence intensity at the microtubule tips to the baseline lattice intensity. EBs comet patterns were obtained from averaging measured fluorescence intensities of line profiles drawn on EBs dashes. A number of MT-comets (100-200) were counted in five to ten cells per condition in each experiment. Image J software was also used to quantify MT density and stability by measuring fluorescence intensity of α-tubulin (total MTs) and α-acetylated tubulin (stable MTs).

Quantification of MT dynamics

To analyze displacements of EB3-GFP, *Manual tracking* plugging of Image J free software was used. Different parameters of MT dynamics related to growing MTs (marked by EB3-GFP) were quantified and analyzed, such as: MT growth speed, duration of MT growth events and MT pausing (numbers and duration). Quantification of the direction of movement of EB3-GFP comets (forwards, backwards and across) was measured as described (Purro et al., 2008)

Statistical analysis

Sets of three to five experiments were performed in each case. All statistical tests and graphing were done using GraphPad Prism5 and SPSS-17 software. Statistical analysis was performed using parametric (Student t) and non-parametric (Mann-Whitney) tests

depending on normality of the data sets (assessed by Shapiro-Wilk test), with a significance level of $p \leq 0.05$. *P*-values are indicated in the graphs: $P < 0.05$ was considered to indicate a statistically significant difference (*= $p < 0,05$; **= $p < 0,005$ and, ***=$p<0,0005$, as stated in bar graphs). All data were expressed as the mean ± standard error (SEM).

Supplementary figure legends

Figure S1. Overexpression of moderate levels of tau does not displace EB1 from MT plus-ends.

A. Confocal pictures of N1E-115 cells transfected with low to medium levels of GFP-tau (green) and stained with an anti-EB1 antibody (red). Scale bar=10μm. Insets show details of EB1-comets in a control (non-transfected) (**a**) versus a GFP-tau transfected cell (**a´**). Average number of EB1-comets per 100μm^2 (± SEM) **(B**) and average length of EB1 comets **(C)** in control cells and cells transfected with GFP-tau. **D**. Quantification of the average fluorescence intensity (± SEM) of the whole MT network (α-tubulin) and of stable MTs (α-Acetylated-tubulin) in control and GFP-tau-expressing cells. Transfected cells presented no significant changes in MT density and a slight increase in MT stability.

Figure S2. Overexpression of EB1 mimics the MAP1B knockdown phenotype

Confocal pictures of N1E-115 cells transfected with low (**A**), medium (**B**) or high (**C**) levels of EB1-GFP (green) and stained with an anti-α-tubulin antibody (red). Scale bar=10μm. While in low expressing cells, EB1 localizes at MT plus-ends (comet pattern, **A**) in medium to high-expressing cells, EB1 interacts with MT segments (**B**) or along the MT lattice (**C**). Interaction of EB1 with MTs is enhanced when its effective concentration is increased in the cell.

Figure S3. Stable downregulation of tau does not enhance binding of EB1/3 to MTs.

N1E-115 stable cell lines were generated by lentiviral infection with either scramble shRNA (control) or different specific tau-shRNAs (1, 2, or a pool of 1+2). **A**. Reduction of tau levels was confirmed by Western blot. β-actin was used as a loading control. **B.**

Confocal immunofluorescence pictures of control and tau-silenced cells, co-stained with anti-tau (red) and anti-EB1 (green).. Details of EB1 comets are shown in insets. **C.** Confocal images of control and tau-depleted cells, stained with anti-tau (red) and anti-α-tubulin (green). Scale bars=10μm. Insets show details of the MT lattice at the cell cortex of control (**c**) and tau-depleted cells (**c´**). MT density is substantially reduced in tau-silenced cells.

Figure S4. Nocodazole induces displacement of EBs from MTs and enhances the interaction between MAP1B and EB3.

Serum-starved N1E-115 cells were treated (or not) with Nocodazole (10 μM, 20 min.). Cells rounded up upon treatment. **A.** Confocal pictures show cells stained with antibodies against α-Acetylated tubulin (green), α-Tyrosinated tubulin (red) and β3-tubulin (blue). Nocodazole induces a complete MT depolymerization. **B.** Immunofluorescence pictures show co-staining for EB1 (red) and EB3 (green) in non-treated versus Nocodazole-treated cells. EB comets disappeared upon treatment. **C.** Nocodazole led to enhanced colocalization of EB3 and MAP1B at the cytoplasm close to the cell cortex of Nocodazole-treated cells.

Figure S5. Proline-directed kinases regulate the interaction between MAP1B and EB3.

A. N1E-115 cells were transfected with GFP or EB3-GFP and serum-starved overnight. Cells were treated (or not) with inhibitors of different kinases, such as GSK-3 (Lithium, 20mM, 3h), CK2 (DMAT, 10μM, 3h) and Cdk5 (Roscovitine, 20μM, 3h) and co-IP assays were performed using an antibody against MAP1B (N-t). Inhibition of proline-directed kinases (GSK-3 and Cdk5) increased the interaction between MAP1B and EB3-GFP. **B.** Colocalization of endogenous MAP1B and EB3 is enhanced upon Roscovitine treatment (10μM, 3h).

Figure S6. An N-t cytosolic fragment of MAP1B sequesters EB1 in the cytosol.

N1E-115 cells were transfected with a construct encoding a Myc-tagged deletion fragment of MAP1B (aa 1-508). Confocal pictures of cells transfected with MAP1B-1-508-Myc show that this N-t MAP1B fragment is diffusely distributed in the cytosol (anti-Myc, red, in **A** and **B**). MAP1B 1-508-Myc expressing cells show a diffuse

cytoplasmic localization of EB1 (anti-EB1, green, **A**) and an unaffected MT lattice (anti-α-tubulin, blue, **B**)**. C**. Quantification of fluorescence intensity of the MT network in control (non-transfected) and MAP1B 1-508-Myc-transfected cells. EB1 comet number per 100μm^2 **(D)** and comet length **(E**) in non-transfected, MAP1B-full length (FL)-Myc and MAP1B 1-508-Myc transfected cells.

Figure S7. MAP1B overexpression slows down EB3-GFP mobility

N1E-115 cells were transfected with EB3-mCherry and either GFP (depicted as EB3-mCherry, white bar) or MAP1B-GFP (black bar). Cells were serum-starved overnight and the EB3-mCherry signal was bleached in a defined ROI located in distal neurites. Fluorescence recovery (FRAP) was followed for 50 sec. Three independent sets of experimental data were normalized and fitted with a two-phase exponential equation. Average k (sec^{-1}) and $t_{1/2}$ (sec) parameters (±SEM) obtained from data fitting are shown in **A** and **B**. Overexpression of MAP1B provokes a slight delay in fluorescence recovery of EB3-mCherry.

Figure S8. Nocodazole delays fluorescence recovery of EB3-GFP in MAP1B-deficient neuronal cells

A and **B**. Curves represent fitting of experimental data obtained from three different sets of FRAP assays performed in distal neurites of either N1E-115 control cells (scramble, in **A**) or MAP1B-depleted cells (MAP1B-shRNA pool, in **B**). Cells were transfected with EB3-GFP, serum-starved overnight, and treated with low doses of Nocodazole (10nM, 1 h). Bleaching was performed in a defined ROI in distal neurites. Fluorescence recovery was followed during 50 sec. Cloud of dots (grey) represents all experimental data taken at every given time point; green lines show average fluorescence; black dotted-lines are SEM of the average, and red lines represent the fitted curves. **C.** Average fluorescence values obtained in **A** and **B** are represented together.

Figure S9. MAP1B-depletion leads to a reduction in MT pausing in neuroblastoma cells.

Control (scramble) and MAP1B-knocked-down (MAP1B-shRNA pool) stable N1E-115 cells were transfected with EB3-GFP and serum-starved overnight. EB3-GFP comets displacements were followed using Manual tracking plugging from Image J software.

Number of pauses per 100 displacements of EB3-GFP was counted. Bar graph shows that MAP-depleted cells present a significantly reduced number of pauses as compared to control cells.

Figure S10. ***Map1b*-/- neurons present a decrease in dynamic and an increase in stable MTs, predominantly at growth cones.**

Immunofluorescence pictures of wt and MAP1B-deficient neurons stained with antibodies against α-Tyrosinated-tubulin (dynamic MTs) or α-detyrosinated (Glu)-tubulin (stable MTs). *Map1b*-/- neurons present shorter axons tipped by enlarged growth cones, filled by looped MTs. In wt neurons, stable MTs enter only the central (C) region of the growth cones, whereas in mutant neurons, stable MTs penetrate also the peripheral (P) region of broad growth cones.

Figure S11. Deficiency of MAP1B -but not of tau- enhances interaction of EBs with MTs in neurons

A. Confocal pictures showing localization of endogenous MAP1B (red), EB1 (green) and β3-tubulin (blue) in 1DIV wt primary hippocampal neurons. **B.** Quantification of average length of comets stained with different antibodies against CLIPs, EB1 or EB3, throughout wt or MAP1B-deficient neurons. **C.** Confocal pictures of 1DIV wt and tau-/- neurons stained with anti-tau (red) and anti-EB3 (green). Insets show normal EB3 comet staining in growth cones of *Tau-/-* neurons.

Figure S12. Enhanced binding of EB3-GFP to looping MTs in MAP1B-deficient neurons

Embryonic wt and *Map1b*-/- primary hippocampal neurons were cultured and transfected with EB3-GFP four hours after plating. 24 hours later, cells were recorded by time-lapse confocal microscopy and EB3-GFP displacements were followed and analyzed. Pictures were taken every second (1sec). **A.** Representative examples of growth cones of wt **(A)** and *Map1b*-/- neurons **(B)**. Snapshots show still images in each case and Z-Max-Projections represent the maximal projection of the images taken. Inverted grey scale snapshots and projections are shown to visualize EB3-GFP comets and trajectories more clearly. Insets with details of EBs-GFP comets displacements are shown in **A** and **B**. In wt neurons (**A**), EB3-GFP comets, and therefore growing MTs, enter the growth cone in a parallel straight array, penetrating some protruding filopodia.

In MAP1B-deficient neurons (**B**), MTs are looped in the growth cone with EB3-GFP showing some plus-end binding as well as MT-lattice interaction.

Supplementary movies legends

Movie S1. EB3-GFP time-lapse in control (scramble) N1E-115 stable cells. Stable scramble cells were transfected with EB3-GFP and serum-starved overnight. Recordings were performed every 2 sec of 30 frames. Figure 6A shows still images, Z-Max-projection and insets with details of EB3-GFP comets displacements.

Movie S2. EB3-GFP time lapse in stably MAP1B-depleted N1E-115 cells. N1E-115 cells stably-depleted of MAP1B (using a pool of specific shRNAs) were transfected with EB3-GFP and serum-deprived overnight. Movie shows 30 pictures taken every 2 sec. Figure 6A shows still images, Z-Max-projection and insets with details of EB3-GFP comets displacements.

Movie S3. Time-lapse of EB3-GFP displacements in the growth cone of a 1DIV wt hippocampal neuron. wt neurons were transfected with EB3-GFP four hours after plating. Recordings of EB3-GFP displacements were performed 24 hours later. Pictures were taken every sec. Still images, Z-Max-projection and insets with details of EB3-GFP comets movements are shown in Figure 8A.

Movie S4. **Time-lapse of EB3-GFP comets in the growth cone of a 1DIV *Map1b*-/- hippocampal neuron.** *Map1b*-/- neurons were transfected with EB3-GFP four hours after plating. Recordings of EB3-GFP displacements were performed 24 hours later. Pictures were taken every sec. Still images, Z-Max-projection and insets with details of EB3-GFP comets displacements are shown in Figure 8B.

Movie S5. EB3-GFP comets penetrate in a straight array into filopodia in growth cones of wt neurons. wt neurons were transfected with EB3-GFP four hours after plating. Recordings of EB3-GFP displacements were performed 24 hours later. Pictures were taken every sec. Still images, Z-Max-projection and insets with details of EB3-GFP comets displacements are shown in Figure S12A

Movie S6. EB3-GFP accumulates at MT plus-ends and lattice of looping MTs in the growth cone of MAP1B-deficient neurons. *Map1b*-/- neurons were transfected with EB3-GFP four hours after plating. Recordings of EB3-GFP displacements were

performed 24 hours later. Pictures were taken every sec. Still images, Z-max-projection and insets with details of EB3-GFP comets displacements are shown in Figure S12B.

Supplementary references

Coquelle, F.M., Caspi, M., Cordelieres, F.P., Dompierre, J.P., Dujardin, D.L., Koifman, C., Martin, P., Hoogenraad, C.C., Akhmanova, A., Galjart, N., De Mey, J.R. and Reiner, O. (2002) LIS1, CLIP-170's key to the dynein/dynactin pathway. *Mol Cell Biol*, **22**, 3089-3102.

Hoogenraad, C.C., Akhmanova, A., Grosveld, F., De Zeeuw, C.I. and Galjart, N. (2000) Functional analysis of CLIP-115 and its binding to microtubules. *J Cell Sci*, **113 (Pt 12)**, 2285-2297.

Komarova, Y., Lansbergen, G., Galjart, N., Grosveld, F., Borisy, G.G. and Akhmanova, A. (2005) EB1 and EB3 control CLIP dissociation from the ends of growing microtubules. *Mol Biol Cell*, **16**, 5334-5345.

Komarova, Y.A., Akhmanova, A.S., Kojima, S., Galjart, N. and Borisy, G.G. (2002) Cytoplasmic linker proteins promote microtubule rescue in vivo. *J Cell Biol*, **159**, 589-599.

Purro, S.A., Ciani, L., Hoyos-Flight, M., Stamatakou, E., Siomou, E. and Salinas, P.C. (2008) Wnt regulates axon behavior through changes in microtubule growth directionality: a new role for adenomatous polyposis coli. *J Neurosci*, **28**, 8644-8654.

Smith, D.B. and Johnson, K.S. (1988) Single-step purification of polypeptides expressed in Escherichia coli as fusions with glutathione S-transferase. *Gene*, **67**, 31-40.

Stepanova, T., Slemmer, J., Hoogenraad, C.C., Lansbergen, G., Dortland, B., De Zeeuw, C.I., Grosveld, F., van Cappellen, G., Akhmanova, A. and Galjart, N. (2003) Visualization of microtubule growth in cultured neurons via the use of EB3-GFP (end-binding protein 3-green fluorescent protein). *J Neurosci*, **23**, 2655-2664.

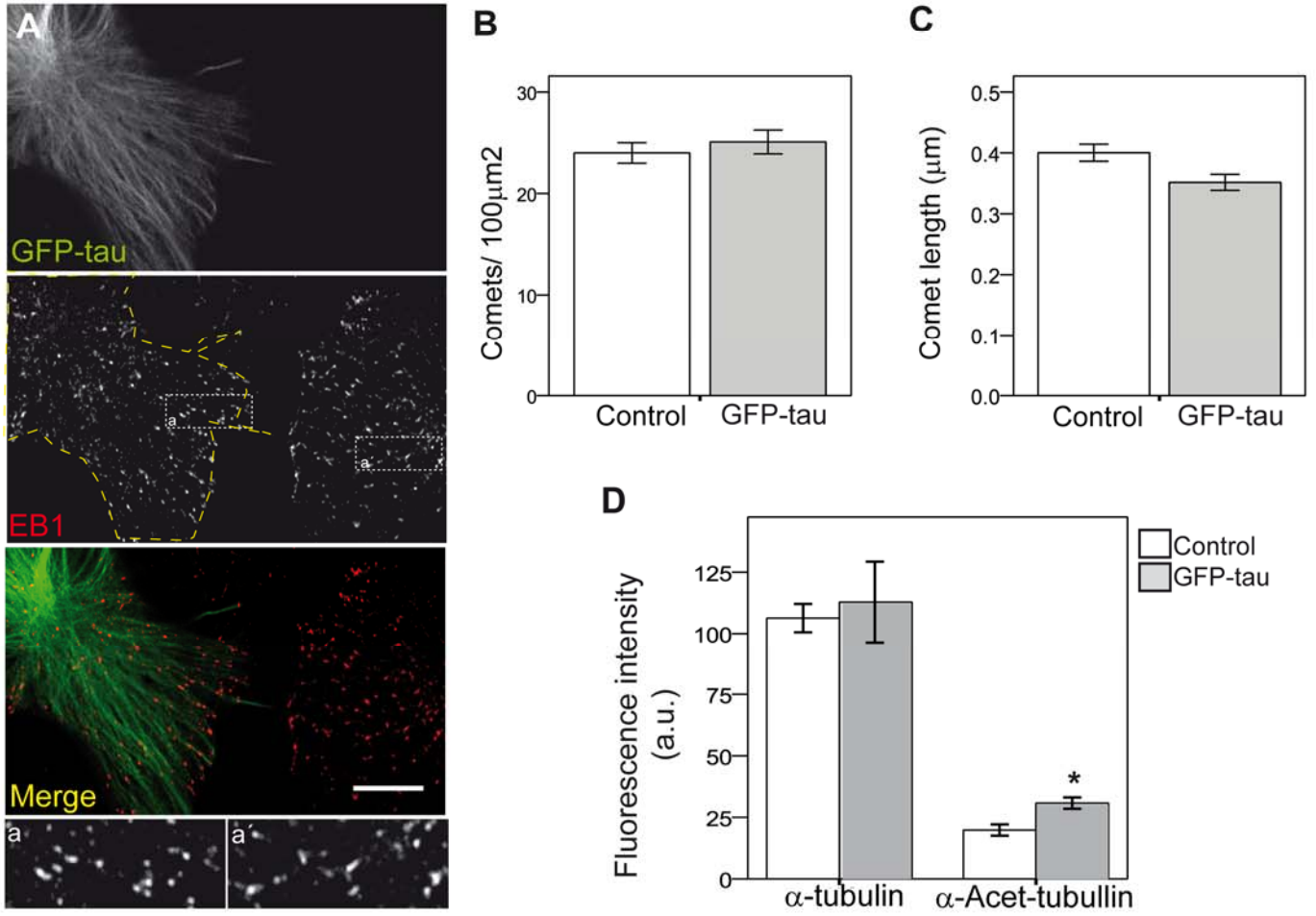
A
GFP-tau
EB1
Merge
a
a'
B
Comets/ 100µm2
30
20
10
0
Control
GFP-tau
C
Comet length (µm)
0.5
0.4
0.3
0.2
0.1
0.0
Control
GFP-tau
D
Fluorescence intensity (a.u.)
125
100
75
50
25
0
*
α-tubulin
α-Acet-tubullin
Control
GFP-tau

Figure S1

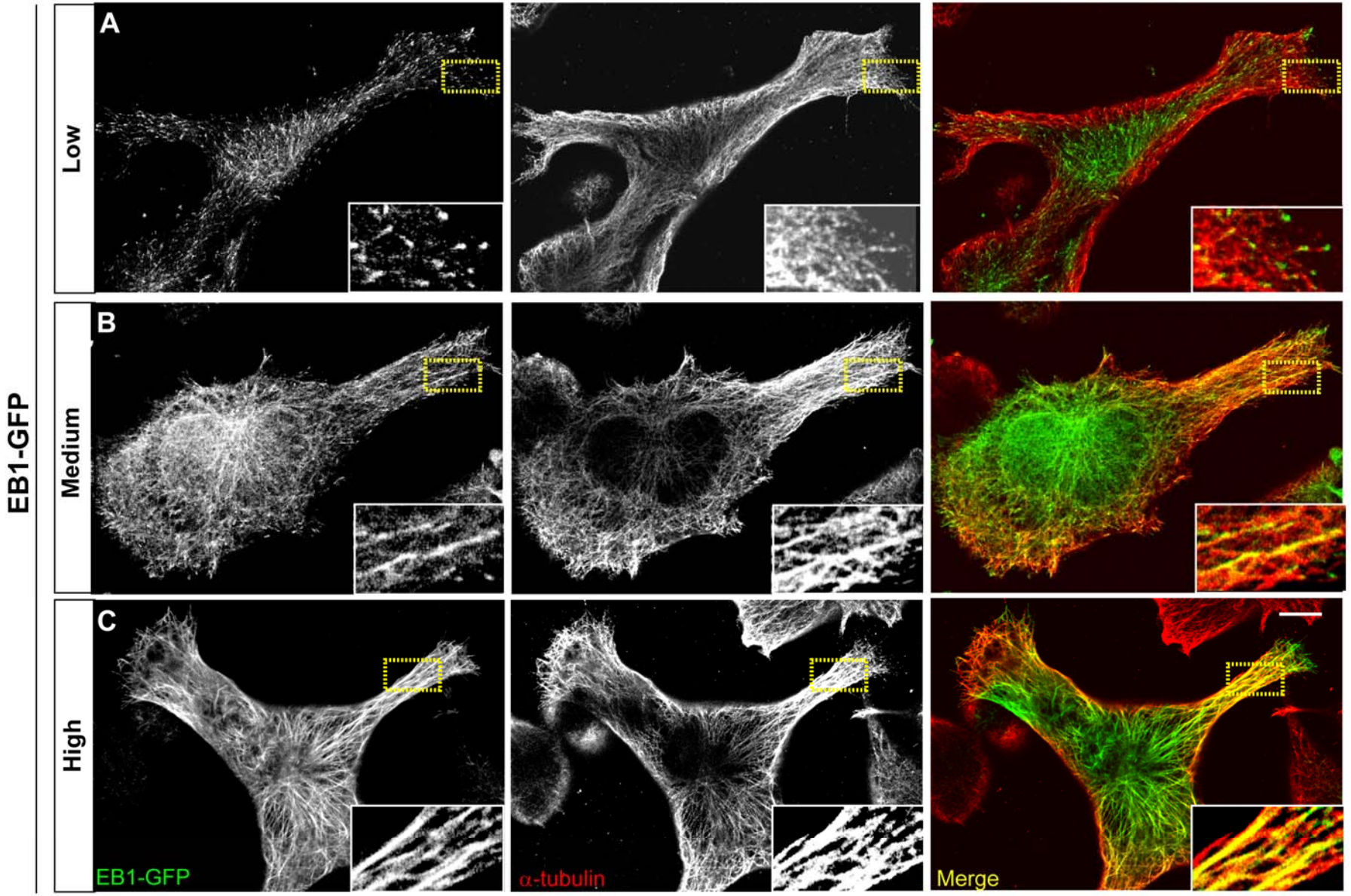

Figure S2

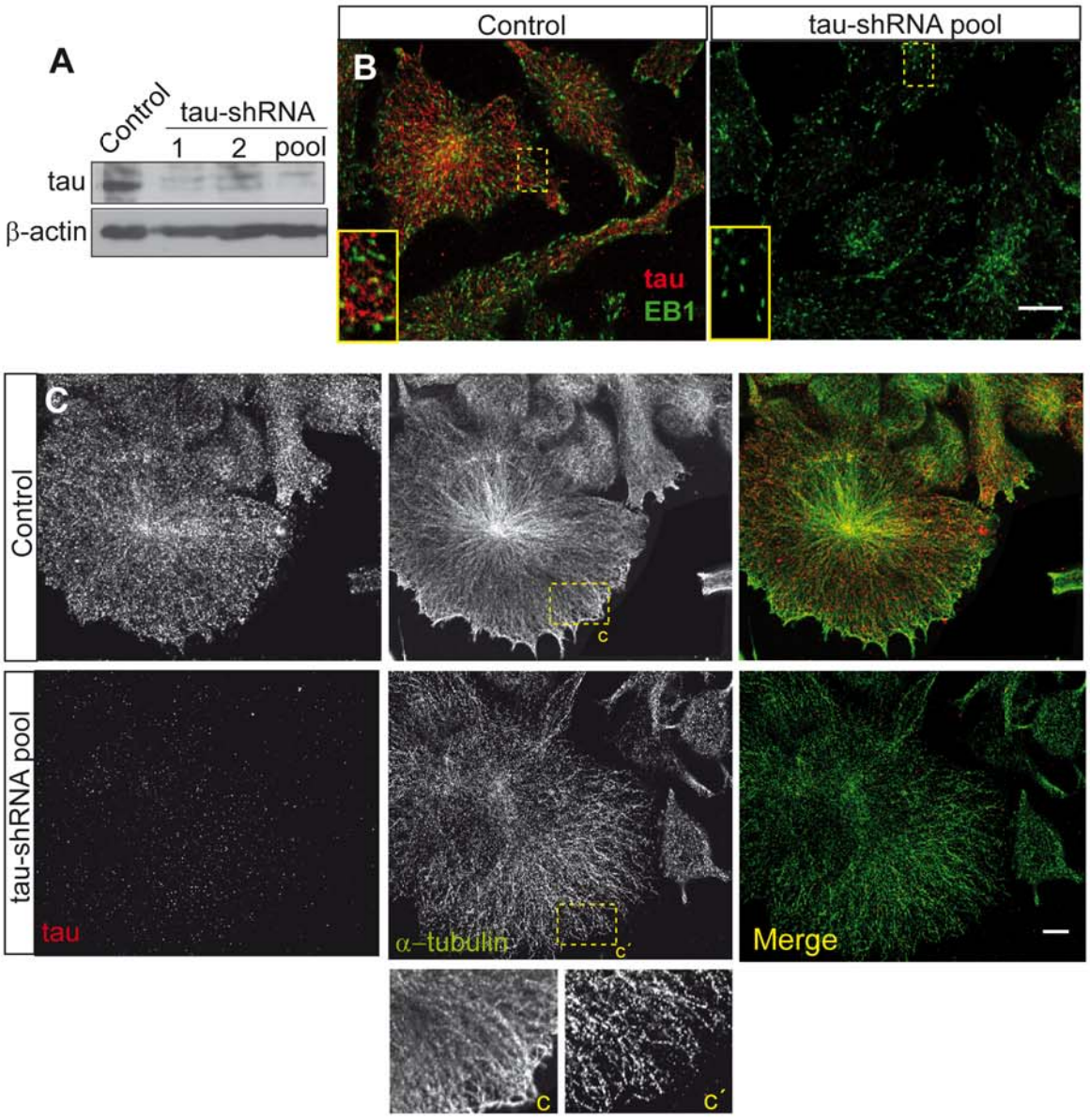
A
Control
tau-shRNA
1
2
pool
tau
β-actin
Control
tau-shRNA pool
B
tau
EB1
C
Control
c
tau-shRNA pool
tau
α–tubulin
c´
Merge
c
c´

Figure S3

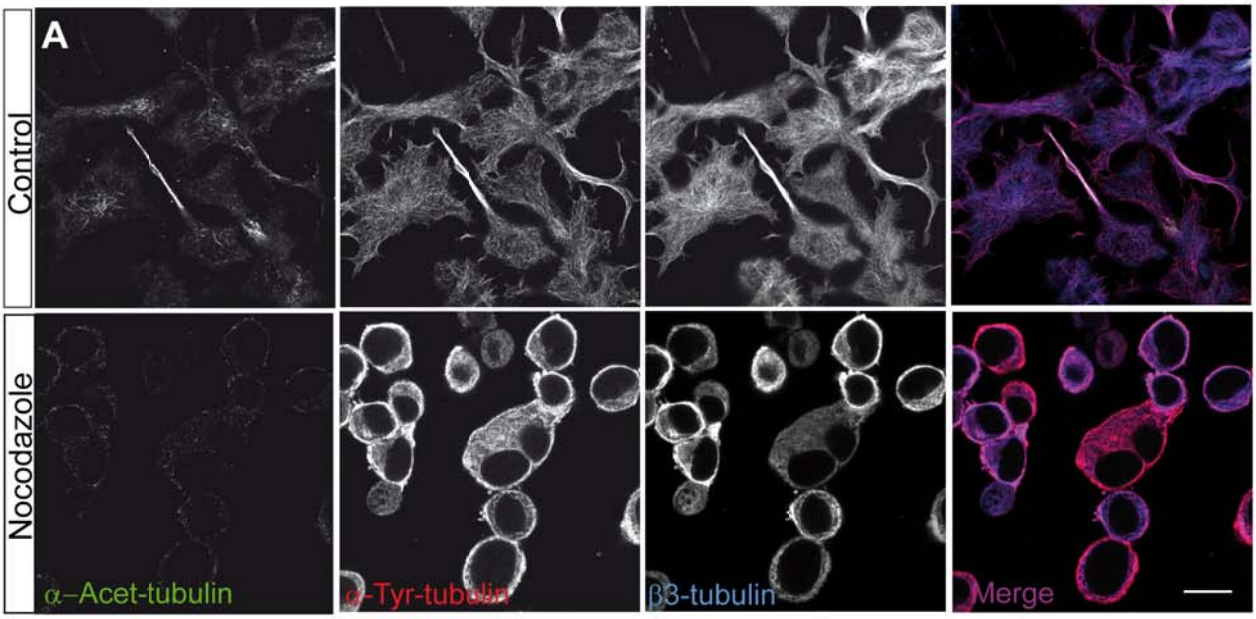
A
Control
Nocodazole
α–Acet-tubulin
α-Tyr-tubulin
β3-tubulin
Merge

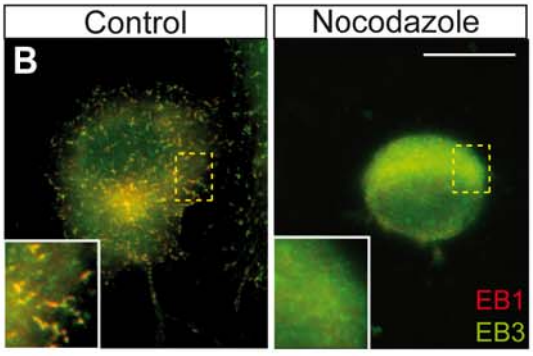
Control
Nocodazole
B
EB1
EB3

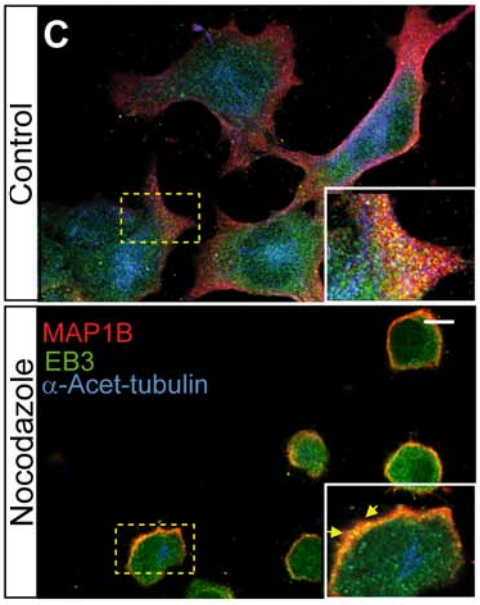
C
Control
Nocodazole
MAP1B
EB3
α-Acet-tubulin

Figure S4

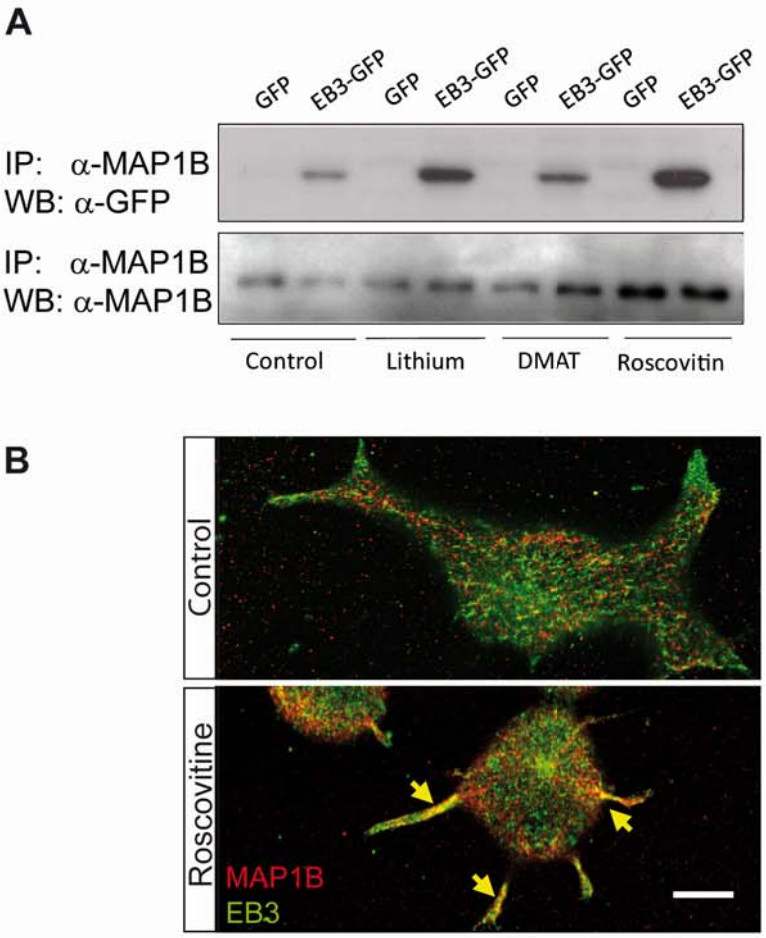
A
GFP
EB3-GFP
GFP
EB3-GFP
GFP
EB3-GFP
GFP
EB3-GFP
IP: α-MAP1B
WB: α-GFP
IP: α-MAP1B
WB: α-MAP1B
Control
Lithium
DMAT
Roscovitin
B
Control
Roscovitine
MAP1B
EB3

Figure S5

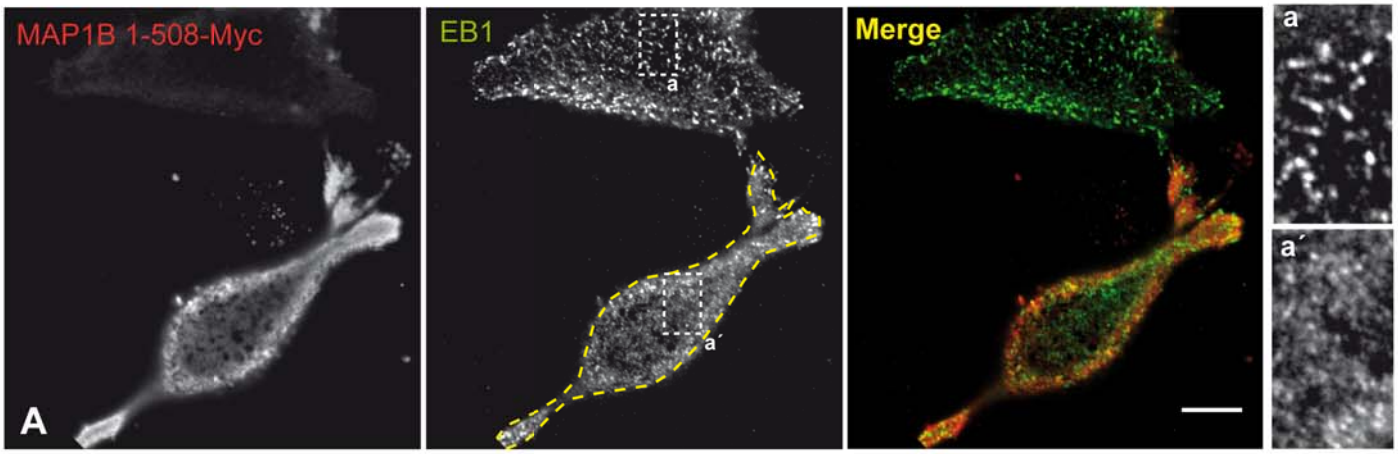
MAP1B 1-508-Myc
EB1
Merge
a
a´
A

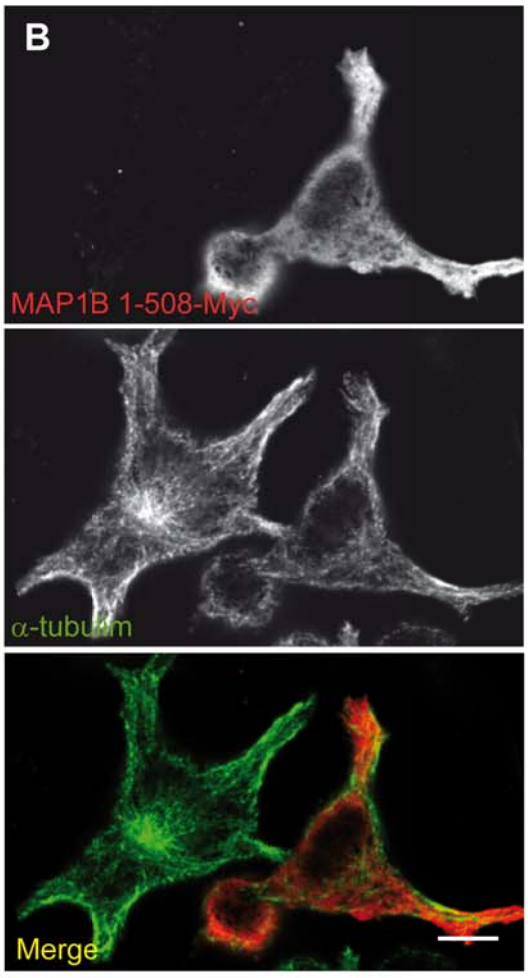
B
MAP1B 1-508-Myc
α-tubulin
Merge

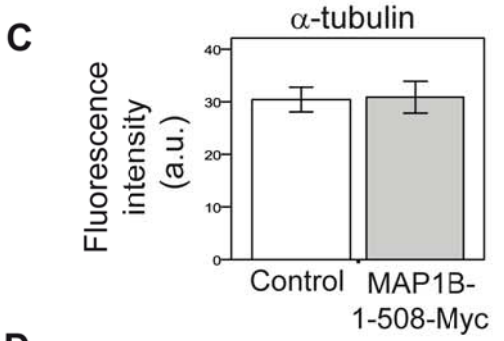
C
α-tubulin
Fluorescence intensity (a.u.)
40
30
20
10
0
Control
MAP1B-1-508-Myc

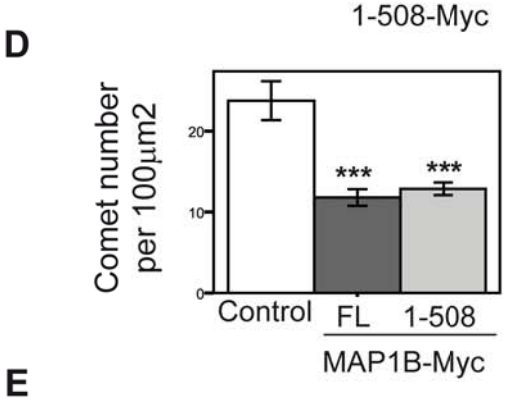
D
Comet number per 100μm2
20
10
0
***
***
Control
FL
1-508
MAP1B-Myc

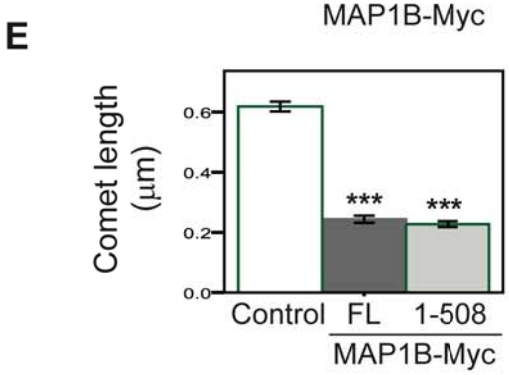
E
Comet length (μm)
0.6
0.4
0.2
0.0
***
***
Control
FL
1-508
MAP1B-Myc

Figure S6

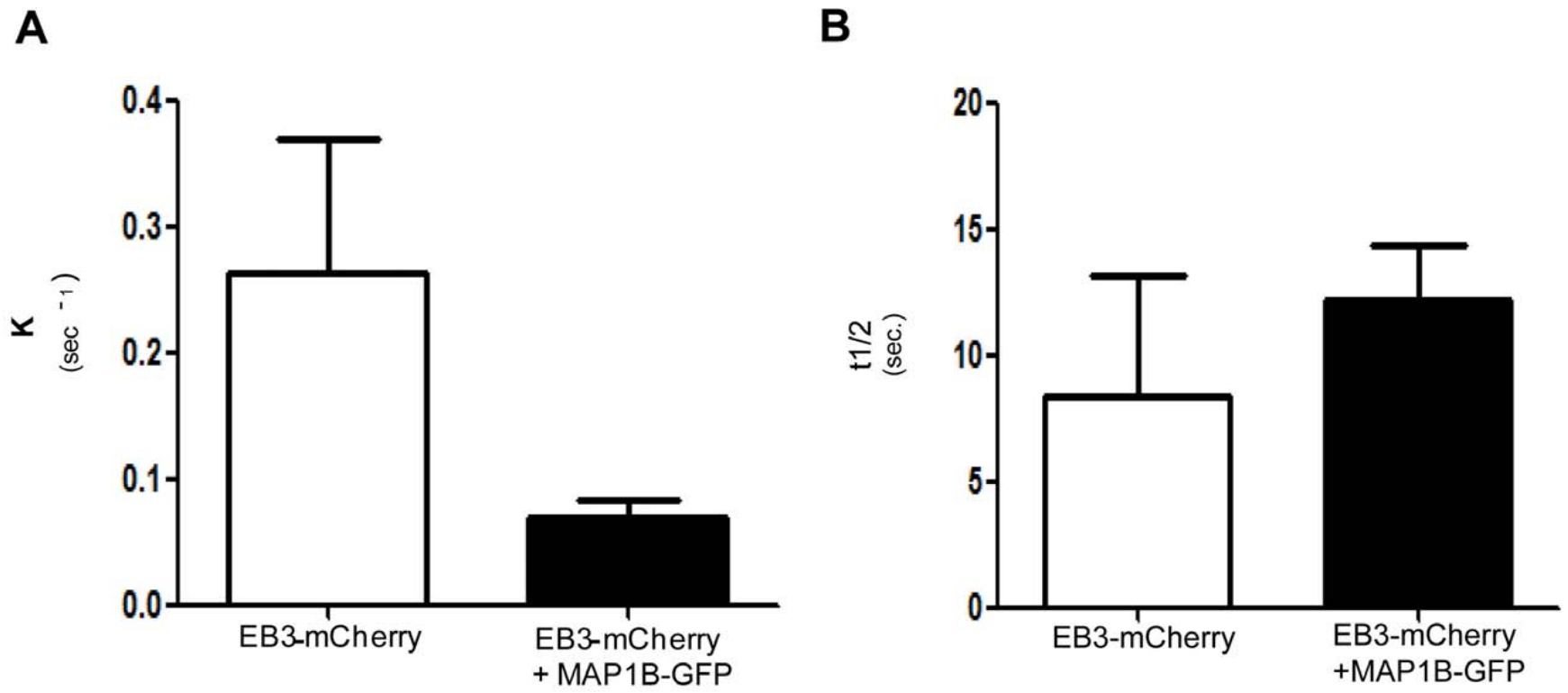
A
K
(sec -1)
0.4
0.3
0.2
0.1
0.0
EB3-mCherry
EB3-mCherry
+ MAP1B-GFP
B
t1/2
(sec.)
20
15
10
5
0
EB3-mCherry
EB3-mCherry
+MAP1B-GFP

Figure S7

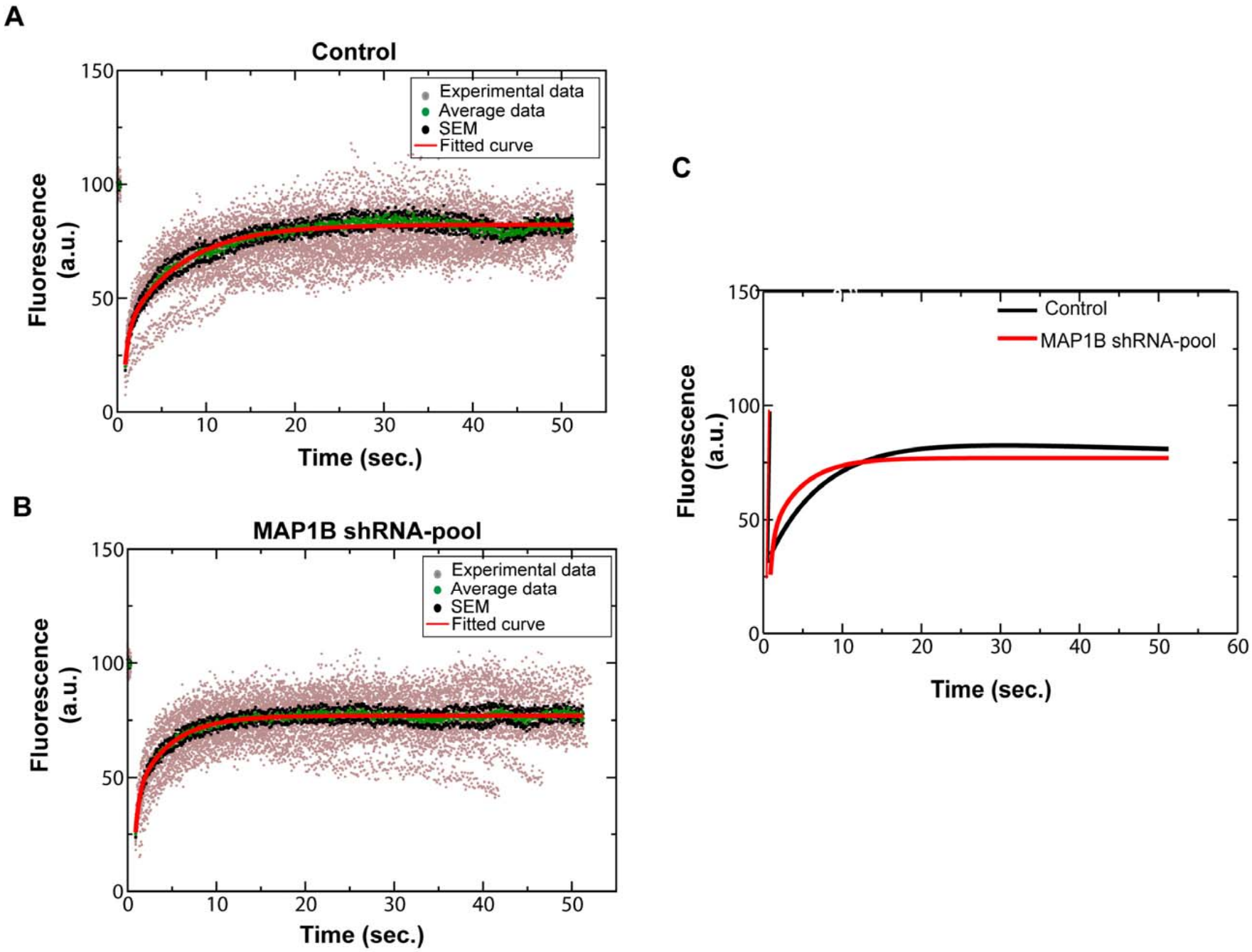
A
Control
Experimental data
Average data
SEM
Fitted curve
Fluorescence (a.u.)
Time (sec.)
B
MAP1B shRNA-pool
Experimental data
Average data
SEM
Fitted curve
Fluorescence (a.u.)
Time (sec.)
C
Control
MAP1B shRNA-pool
Fluorescence (a.u.)
Time (sec.)

Figure S8

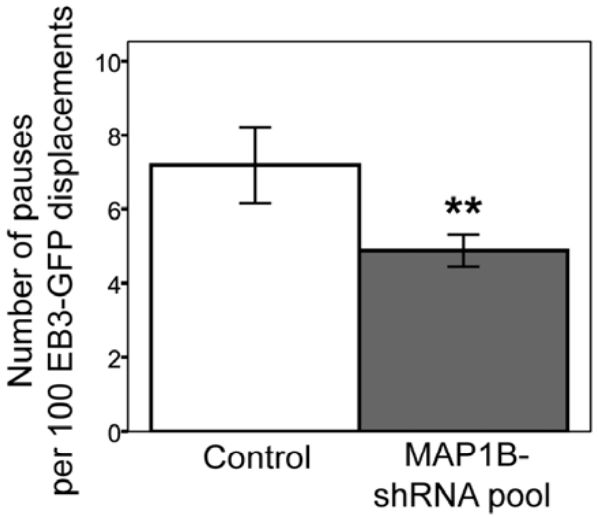
Number of pauses
per 100 EB3-GFP displacements
10
8
6
4
2
0
**
Control
MAP1B-
shRNA pool

Figure S9

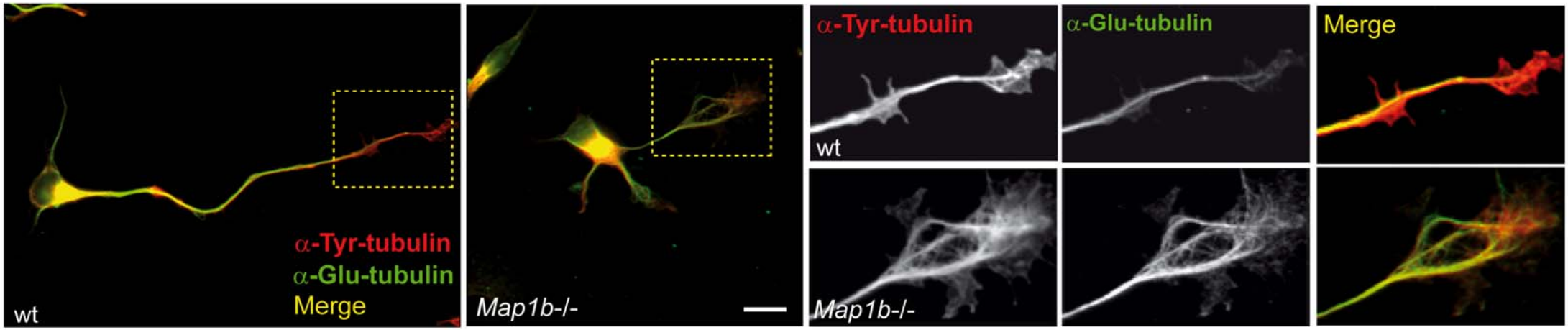
α-Tyr-tubulin
α-Glu-tubulin
Merge
wt
Map1b-/-
α-Tyr-tubulin
α-Glu-tubulin
Merge
wt
Map1b-/-

Figure S10

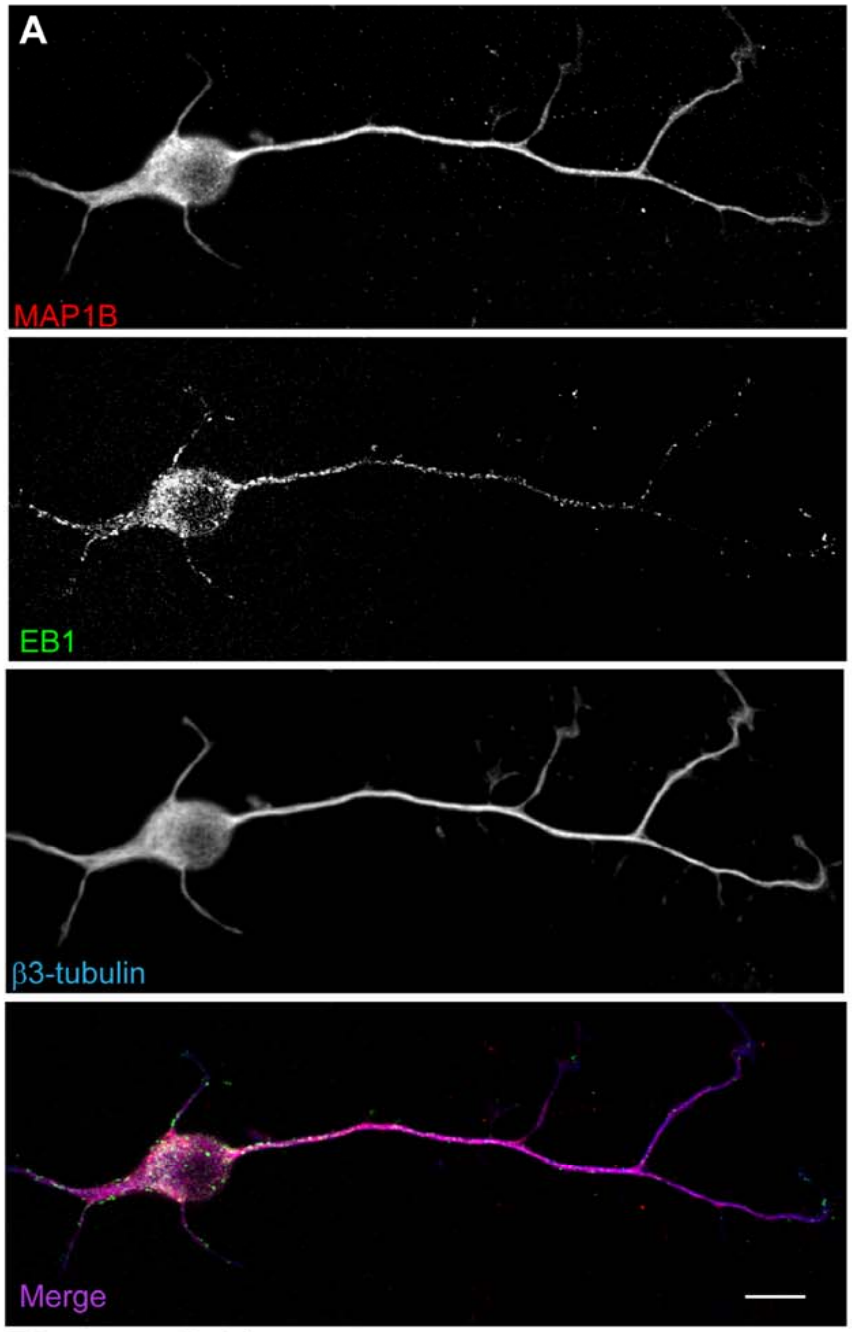
A
MAP1B
EB1
β3-tubulin
Merge

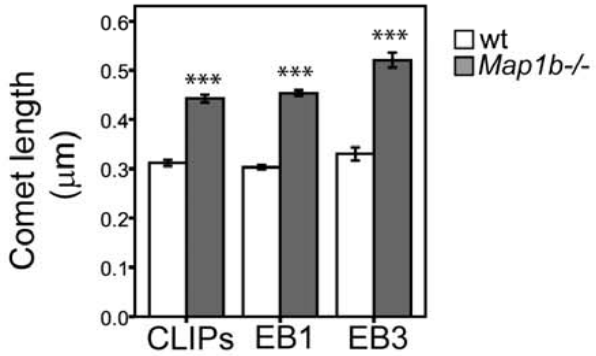
B
Comet length (μm)
0.0
0.1
0.2
0.3
0.4
0.5
0.6
***
***
***
CLIPs
EB1
EB3
wt
Map1b-/-

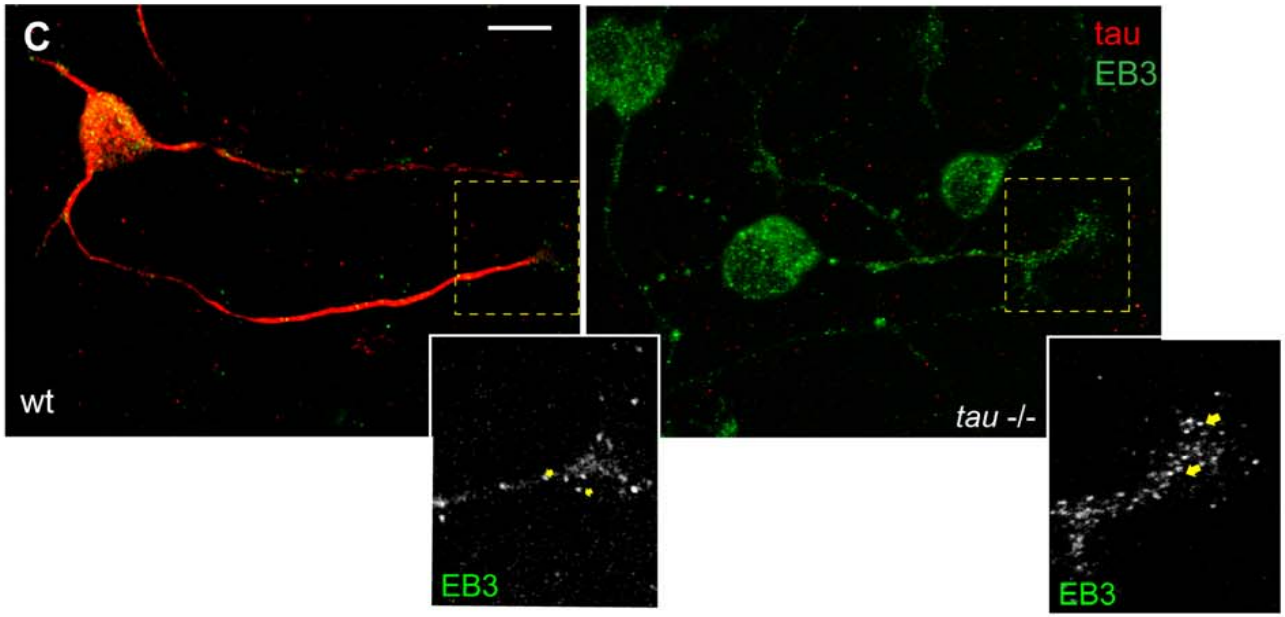
C
wt
tau
EB3
tau -/-
EB3
EB3

Figure S11

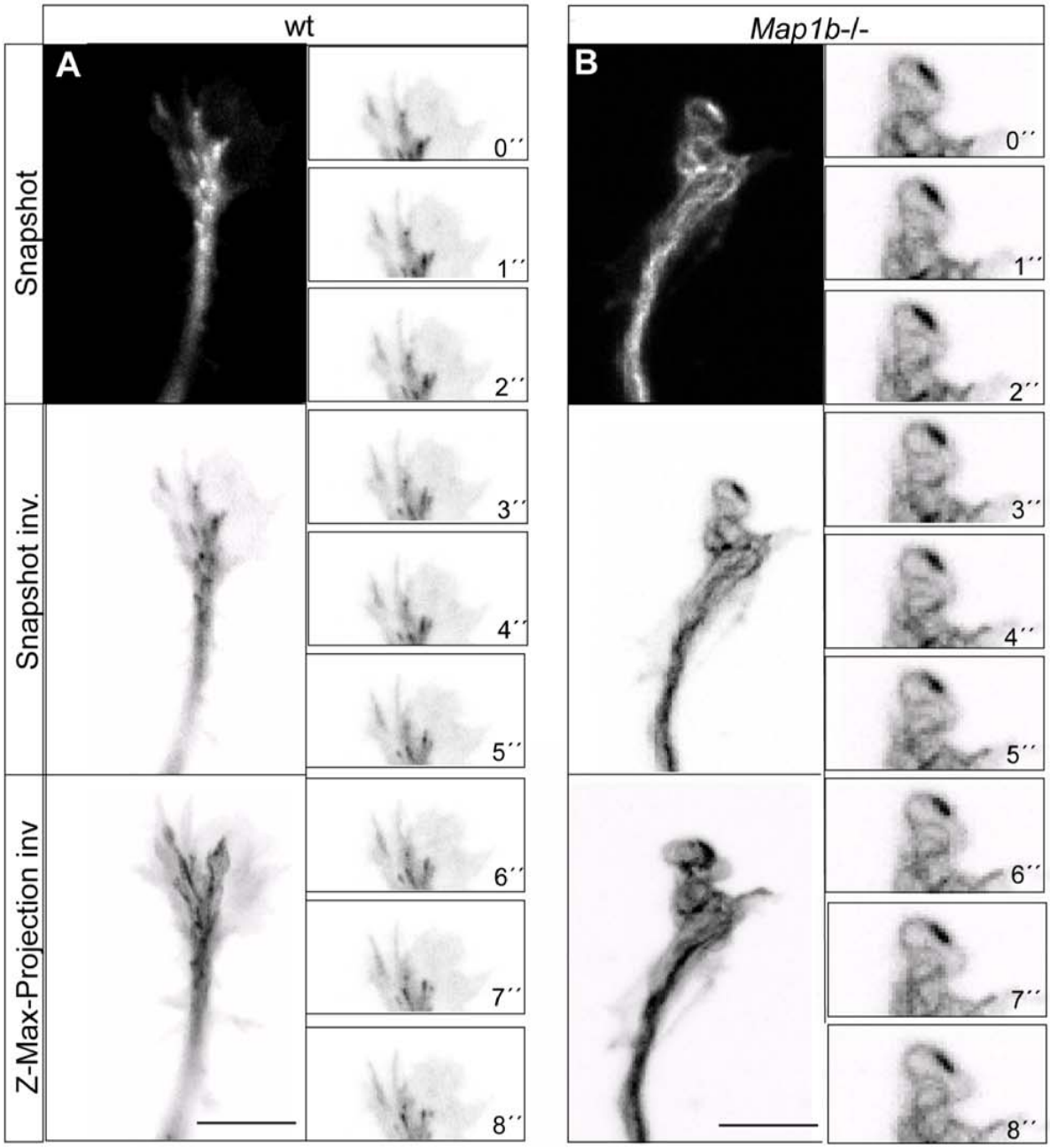
wt
Map1b-/-
A
B
Snapshot
Snapshot inv.
Z-Max-Projection inv
0´´
1´´
2´´
3´´
4´´
5´´
6´´
7´´
8´´

Figure S12